Image-based operational modal analysis and damage detection validated in an instrumented small-scale steel frame structure

Cecilia Rinaldi[a,*], Jacopo Ciambella[b], Vincenzo Gattulli[b]

[a] *DICEAA, University of L'Aquila, via G. Gronchi 18, 67100, L'Aquila, Italy*
[b] *DISG, Sapienza – University of Rome, via Eudossiana 18, 00184, Rome, Italy*

Abstract

The use of image-based techniques in structural dynamics is constantly growing thanks to the decrease in the cost of high-speed cameras and the improvement in image processing algorithms. Compared to traditional sensors, such as accelerometers or velocimeters, the use of fast cameras for data acquisition allows the number of measurements points to be significantly increased. However, this abundance of points, not always lead to an increased accuracy of damage detection algorithms. In this paper, we compare different damage detection techniques by using modal quantities of a small scale steel frame obtained from measurements acquired through a high-speed camera with different image processing techniques. The Hybrid Lagrangian Particle Tracking (HLPT) algorithm and Digital Image Correlation (DIC) are both used to extract displacement measurements from images. The results are compared with those obtained with seismic class accelerometers which are normally used in the lab for such an application. Damage localization and intensity have been determined by using image-based measuremets with the same accuracy obtained by a more common approach.

Keywords: structural health monitoring, digital image correlation, fast camera, experimental validation, time and frequency domain, mode shape,

*Corresponding author
Email address: cecilia.rinaldi@graduate.univaq.it (Cecilia Rinaldi)

mode curvatures, damage detection

1. Introduction

In the field of Structural Health Monitoring (SHM), vision-based techniques have emerged as suitable alternative to traditional sensors as they allow multiple points and contactless measurements [1]. They are non-invasive techniques and do not have the burden of modifying the dynamics of the structure by adding mass or rigidity to it.

The operating principle of every image based dynamic technique is the comparison of images taken at different times. The number of frames per second that can be recorded is a compromise with the sensor accuracy: lower sensor resolutions would allow higher frame rates, thus higher frequencies of vibrations that can be detected, but would reduce the spatial resolution of the measurements, thus the capability of detecting low amplitude vibrations. High resolution sensors can be used to detect motion of a large scale structure, but with frequency limited to few frames per second. Viceversa, current fast cameras allows the capturing of images of the oder of 10 megapixel at frequencies of up to 1000 Hz [2].

In [3] camera models used in SHM are described and classified in portable, USB web and industrial cameras. A portable camera (e.g. 1920x1080 resolution, 60 fps frame rate) can provide high resolution, be equipped with zoom lens and can be suitably used for close-range measurements. The USB web cameras provide high resolution, low frame rate and they are generally used for close-range measurement since the measurement distance is limited by the use of embedded lenses. They have fixed resolution and frame rate or multiple resolution-frame-rate modes (e.g. 1920x1080 resolution, 30 fps; 1080x720 resolution, 30 fps). Among the others, industrial cameras can provide high frame rates and high resolution, real-time displacement monitoring and image acquisition for post-processing, they are programmable, controlled by computer and can use additional lenses for image acquisition. For industrial cameras only the

maximum frame rate is provided for reference (e.g. 2048x1536 resolution, 120 fps frame rate), but the actual frame rate can be defined by the user. Adjustable region of interest and subsampling features allow lower-resolution output formats at much higher frame rates. For instance, in [4] a high-speed camera with full resolution of 1920x1440 pixels and a frame rate of 500 fps was used to record the in-plane dynamic behaviors of a two-story frame structure, whereas the 3D dynamic behavior of a membrane was captured in [5] by three cameras with 1.3 megapixels and 30 fps.

Over the years, different methods have been proposed to identify the dynamic properties of structures through image based techniques. These methods include point tracking, edge tracking techniques and image blurring.

One of the first attempt to use recorded images to detect the dynamic movement of a structure was proposed in [6]. At that time, the hardware capabilities were limited to 25 fps but spline interpolation was applied to improve the resolution of the measurements, assuming a continuous and smooth character of the dynamic effect.

A point tracking algorithm based on the detection of distinct features was used in [7] for structural identification without the need to install markers. In that work, the corner detection method suggested by Harris and Stephens [8] was applied to extract the features, whereas the Kanade–Lucas–Tomasi (KLT) algorithm [9]allowed the tracking.

In [4] the location of damage in steel frames was conducted using a 500 fps camera. First, they determined the best marker positions and shapes for image processing algorithm, then measured the response of the intact and damaged structures to forced vibrations. Finally, a damage detection algorithm based on modes shape differences was applied to evaluate the damage location. In [10] the problem of inserting markers on the structure was partially solved by using a colour laser. Testing were carried out on a beam-like structure in which target for the image processing algorithm were applied through a laser on both the damaged and the undamaged structure. The damage detection algorithm was based on the modal curvature shape extracted from the frequency response

function with a peak-peaking algorithm.

Although the use of markers on the structure can improve the results of the image processing, there are many practical situations in which access to their free points could be difficult, or the insertion of markers to the structure could be an issue. In these situations, edge detection algorithms can be used [11], [2], [12]. These methods require high image resolutions, and high-contrast, thus they are especially suited for slender structures. In [13], the edge detection algorithm was applied to evaluate the dynamics of an entire cable in a bridge structure, an effort that would have not been feasible by covering the entire cable with markers. A method for detecting the edge of the cable based on the wavelet transform on the images was presented in [14], they eventually detect the location of the cable failure, and compared the results in terms of natural frequencies of the cable extracted by the image processing method and the laser measurement. The Edge detection method was utilized to record vibrations of a simple two-arc beam for obtaining the dynamic characteristics of the healthy and damaged structure by Poudel et al. in [15].

As for the research carried out by McCarthy et al. [16], Image de-blurring technique was used to monitor small scale laboratory models as well as large scale test. Such a technique partially alleviate the inherent compromise that exists when selecting sensors for monitoring of dynamic structures. Instead of capturing vibrations using very high speed imaging, a high-resolution long-exposure photograph is used, in which the localised object image becomes motion blurred. A specialised image registration algorithm would be necessary to make measurements from such a motion blurred image. [17], [18]

Compared to other modal analysis techniques, image-based algorithms have the disadvantage of requiring a high level of expertise to process the acquire data with a long processing time compared to traditional sensors for which the data is often available real-time and onsite. For such a reason a proper comparison of the different image processing techniques should take into account the processing time as an additional figure of merit.

A classification of different visual tracking algorithms along with the feature

tracked is reported in [19].

The *correlation-based template matching* (applied in [20]) is based on a template, a selected Region Of Interest (ROI), which slides across another image to search the best matching. Two major types of methods are used to calculate the similarity between the template and overlapped region of the image for ROI matching and they are the sum of squared differences and the cross-correlation methods. Digital Image Correlation (DIC) also follows these approaches. Unlike the template matching, DIC first divides the whole image into multiple sub-regions with grids and uses template matching to calculate the displacement of the sub-region; the displacement in the whole image is obtained with interpolation techniques. Usually, in dynamic tests only several markers were tracked by using DIC to reduce the computation time.

The *full field dense optical flow* method is used in [21] and it calculates the optical flow for two images by taking on two assumptions, brightness constancy and temporal regularity. Optical flow is the velocity estimation of a video and it is a vector which points from the initial location to the end location of the motion. The method based on *sparse optical flow at feature points* extracts the feature points from image first and then calculate the optical flow. The feature points are a small region (e.g. a sub-image with 5x5 pixels) which is a low sample of target with distinct features (i.e. intensities, gradients in different directions, textures). This techique is used in[22].

In this paper, two image analysis algorithms have been used, DIC and Hybrid Lagrangian Particle Tracking (HLPT) algorithm, which follow respectively the approach of the correlation-based template matching and the sparse optical flow at feature points. Both are applied to the image data acquired during an experimental campaign conducted on a 4-dofs small-scale steel frame structure excited by dynamic actions. The structural response is recorded with accelerometers and with a high-speed camera. The paper [23] reports the direct comparison of image analysis measurements, obtained with HLPT algorithm, with acceleration measurements which confirms that the image analysis turned out to be sufficiently accurate for structural identification purposes. In this

work, the comparison between HLPT and DIC is reported and the advantage of the image-based system, that this a widespread measurement tool, is exploited in the damage detection problem. The damage is introduced by removing the two steel bracing located on the third floor.

The organization of the paper is the following: Section 2 describes the experimental setup, the two algorithms used to process the images and the comparison between these two image analysis results; Section 3 reports the operational modal analysis results obtained from accelerometer and image-based measurements; Section 4 is dedicated to the damage detection problem dealt with accelerometer and image-based measurements.

2. Data extraction

2.1. Experimental setup

Experiments have been carried out at the "Laboratory of Materials and Structures" of Sapienza, University of Rome (Italy), on a spatial model of a 4-story shear type steel (S235) structure with two steel bracings in the inter-story 2-3, indicated as "undamaged structure" in the following. Its height is 800 mm (200 mm for each inter-storey), the plan is squared (300x300 mm), the cross section of columns is rectangular (50x4 mm) and the one of beams is L-shaped (50x50x4 mm). The damage is introduced by removing the bracings and this is indicated as "damaged structure" in the following. Sand (0.3-0.5 mm diameter) was sticked on the structure to create the features to be tracked with the HLPT algorithm and the stochastic pattern to be identified by the DIC algorithm.

Two type of tests were conducted, one with a white noise input (flat in the range of the structural frequencies, 8-100 Hz) provided at the base of the structure by an one-dimensional electrodynamical shaker (Dongling GT700M, slip plate dimension 700x700x45 mm^3), and the other with the structure being hit at the top floor with an instrumented hammer (PCB Piezotronics Modally Tuned ICP model, hammer mass 5.5 kg).

Two acquisition systems were used to record both accelerometric and image-based measurements. The accelerometers used in these tests were seismic class sensors PCB 393A03 and PCB 352C33 with noise density $2\mu g/\sqrt{Hz}$ in the bang 1-5000 Hz. The second acquisition system includes a video camera and a digital recorder of IO Industries. The camera is the Flare 12M125xCL, a high resolution, high-speed area scan camera; the sensor size is 4096x3072, the pixel size 5.5 μm x 5.5 μm and the frame rate at full resolution is 124 fps (8-bit) and 100 fps (10-bit). For this experiments, the frame rate of the camera was set to 200 fps with 320x763 pixel the size of the image. The digital recorder is the CORE2CLPLUS IO DVR, Core 2. The camera is installed in front of the structure to capture images in the motion plane, as sketched in Fig.1. Further details on the experimental setup are reported in [23].

(a) (b) (c)

Figure 1: Experimental setup: a) the steel frame structure mounted on the shaking table; b) the high-speed camera installed in front of the structure to record motion in the plane (x, z); c) sketch of the experimental setup and reference system.

2.2. Image analysis techniques

The displacements of feature points were obtained by two algoritms: the Hybrid Lagrangian Particle Tracking (HLPT) algorithm [24] and the Digital Image Correlation (DIC) technique [25].

The HLPT algorithm is based on the solution of the optical flow equation and selects areas of each image where strong brilliance gradients exist. Such

areas can be associated to feature points and are good features to track from frame to frame. The HLPT algorithm consists in two steps: particle detection and temporal tracking. Through the solution of the image intensity conservation equation, a set of positions, associated with the displacement vector predictor, for which the optimization problem is well-posed, is detected. Those positions are then associated to the centroid coordinates using two 1D Gaussian functions built around the integer position of the local maximum of the intensity value of each detected feature. To identify successive positions of the same particle in the next frames the nearest neighbor principle was employed. Among the candidates, that with the minimum Eulerian distance from the position determined with the displacement predictor was selected. However, this method differs from the 'classical' nearest neighbor one because the solution of the assignment problem is strengthened by using the displacement vector predictor; as such, it is not erroneously influenced by fast moving particles with respect to the mean inter-particle distance. For such a reason, HLPT algorithms are often used in particle hydro-dynamics.

The DIC technique, implemented by using the GOM Correlate software (www.gom.com), is able to evaluate areas via reference point markers or through stochastic image information. In this work, stochastic pattern has been used; the random distribution of image information ensures that an area, usually called subset, can be identified as clearly as possible in its local neighborhood because it is unlikely that a random pattern exists twice in a random neighborhood. The identification of a subset in several images is called matching. Several functions exist to match the subset from one image to another, such as image correlation or the method of least squares.

The algorithms used to process the high-speed camera images return the trajectories of feature points (stochastic pattern), created by attaching sand on beams and columns surfaces. Different points have been sampled along the whole structure obtaining many more measurement points than the accelerometer system acquisition. The comparison between the two image analysis techniques is showed in Fig.2 for a test in which the structure is excited through

an hammer and in Fig.3 for which a shaker test is considered. The results are compared in terms of displacement time histories of fourth floor (DOF 4), as reported in Fig.2a,b and Fig.3a,b, Power Spectral Density (PSD) depicted in Fig.2c an Fig.3c, and mode shapes identified from the image-based signals showed in Fig.2d an Fig.3d. Furthermore, in Tab.1 a computational time comparison is reported; the image analyses have been performed on a Corei7-8th Gen Intel® CPU laptop, with 16GB memory.

Although the results of the feature extraction are practically the same either in terms of time series or power spectra, the DIC algorithm was 2 times faster on the laptop computer used for the test. Therefore, all the subsequent analyses are carried out with DIC data.

Table 1: Image analysis computational time carried out on a Corei7-8th Gen Intel® CPU laptop, with 16GB memory.

	Test duration	Feature points tracking duration	
		HLPT	DIC
Shaker test	110 s	5 h	2 h
Hammer test	14 s	2 h	1 h

3. Image based operational modal analysis

Operational modal analysis (OMA) allows to describe structural dynamics in real operating conditions with unknown excitation. The advantages and drawbacks of such output-only techniques are discussed in [26] where they are applied to extract useful information from rapid dynamic testing of seismically damaged complex buildings. Different procedures, such as Enhanced Frequency Domain Decomposition (EFFD), Eigensystem Realization Algorithm (ERA), Stochastic Subspace Identification (SSI), and Time-Frequency Instantaneous Estimators (TFIE), for identifying both modal and physical models for output-only modal identification are discussed in [27] and their performance are evaluated with the ambient vibration response of a three-dimensional frame structure.

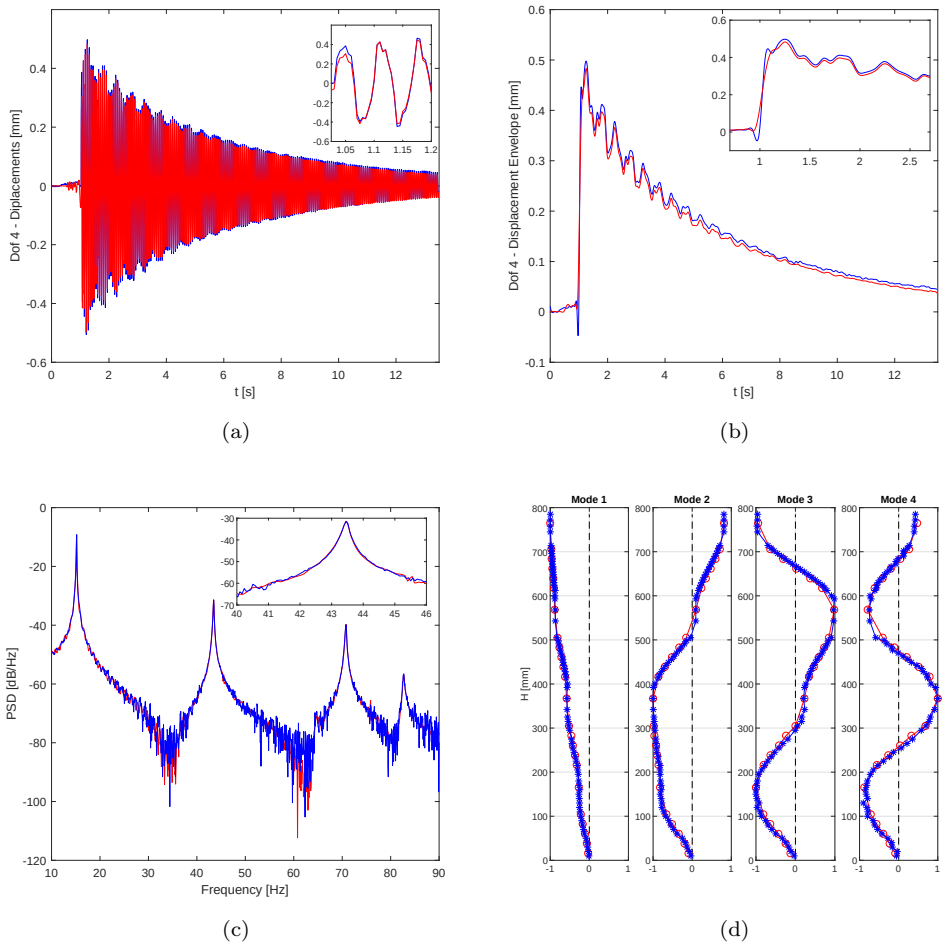

Figure 2: Results of the hammer test executed on the damaged structure obtained with HLPT (red) and DIC algorithm (blue): (a) Displacement time histories of the fourth floor; (b) Displacement envelope; (c) Power Spectral Density (PSD); (d) Mode shapes.

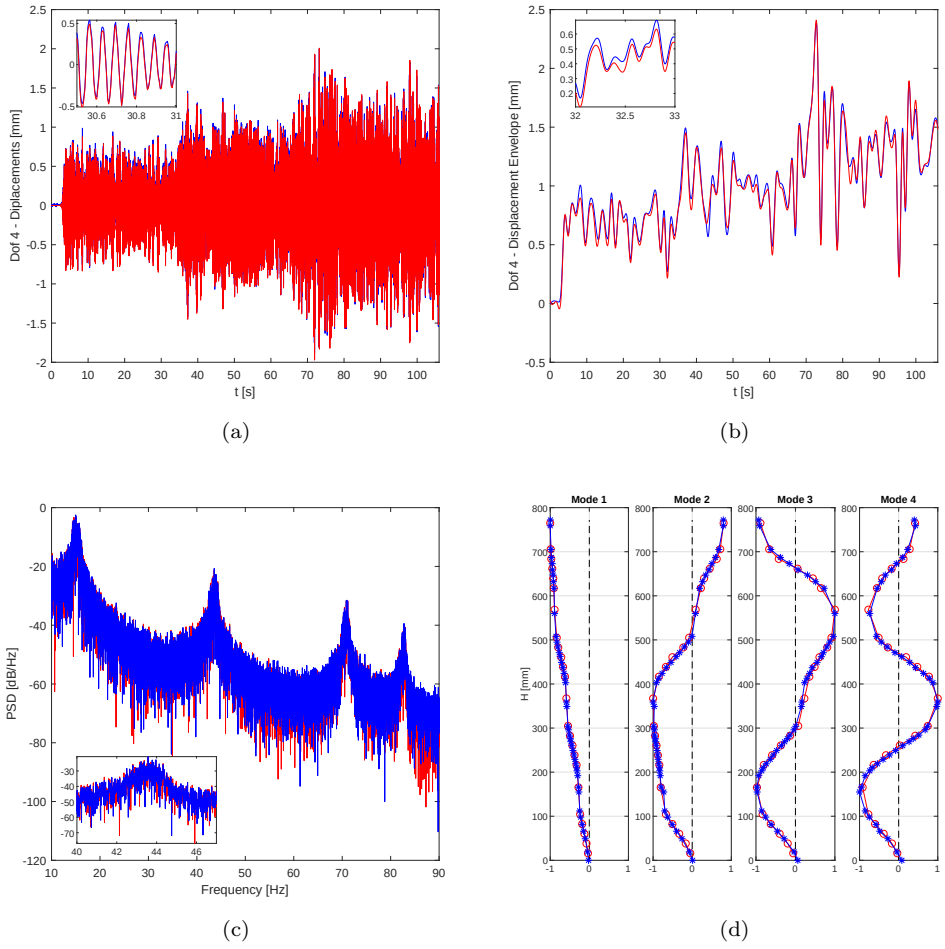

Figure 3: Results of the white noise test executed on the damaged structure obtained with HLPT (red) and DIC algorithm (blue): (a) Displacement time histories of the fourth floor; (b) Displacement envelope; (c) Power Spectral Density (PSD); (d) Mode shapes.

In our work, modal properties of the structure in the undamaged and damaged configuration have been extracted by the Frequency Domain Decomposition (FDD)[28] and Stochastic Subspace Identification (SSI) [29] techniques applied to the results of the white-noise shaker test.

These analysis were conducted by using the displacements of 24 feature points shown in Fig.4 obtained with the DIC algorithm. In addition, 4 accelerometer, one at each floor, were used as comparison.

(a) (b)

Figure 4: Two image samples acquired through the Flare camera. The blue and red dots indicate, respectively, the measurement points extracted in the undamaged and damage configuration of the structure.

The natural frequencies identified with these techniques are listed in Tab.2 for both undamaged and damaged structure. Fig. 5 reports the mode shapes identified with FDD and Fig.6 reports the stabilization diagrams obtained by applying SSI. The natural frequencies identified with SSI from the accelerograms and the image based displacements differ by less than 3% and the ones identified with FDD differ by less than 1%; the image-based mode shapes evaluation is more accurate than the accelerometric one thanks to the higher number of

measurement points available.

Table 2: Modal frequencies extracted through SSI and FDD techniques and from acceleration and displacement measurements.

	Undamaged structure				**Damaged structure**			
	Acceleration		**Displacement**		**Acceleration**		**Displacement**	
Mode	**SSI** [Hz]	**FDD** [Hz]	**SSI** [Hz]	**FDD** [Hz]	**SSI** [Hz]	**FDD** [Hz]	**SSI** [Hz]	**FDD** [Hz]
1	16,7	17,3	17,2	17,2	14,6	14,9	15,1	14,9
2	53,8	54,9	54,9	55,0	42,9	43,9	43,5	43,58
3	71,5	72,9	72,8	72,9	69,5	71,0	70,8	71,1

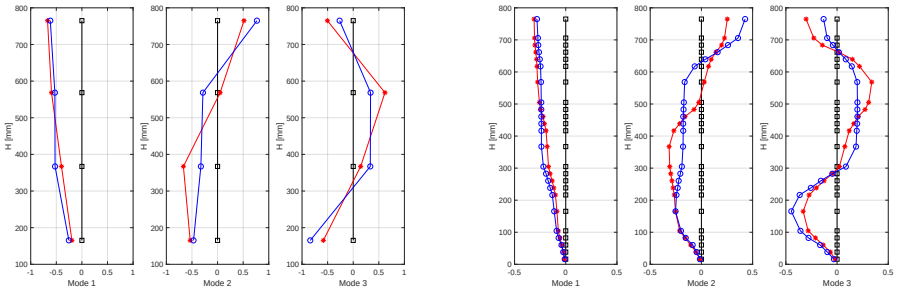

(a) (b)

Figure 5: Mode shapes extracted through the FDD technique from acceleration (a) and displacement (b) measurements.

4. Damage Identification

The focus of this section is the use of the results of the image-based OMA in damage detection procedures. To tackle this problem, several techniques will be compared both in the time and in the frequency domains and the results will allow to highlight advantages and disadvantages of each techniques in terms of accuracy in determining damage location and damage intensity. For example, in [30] two approaches have been used for the monitoring of dynamic systems. Both are based on stochastic subspace identification and take the statistical uncertainties into account. One approach requires a statistical damage indicator

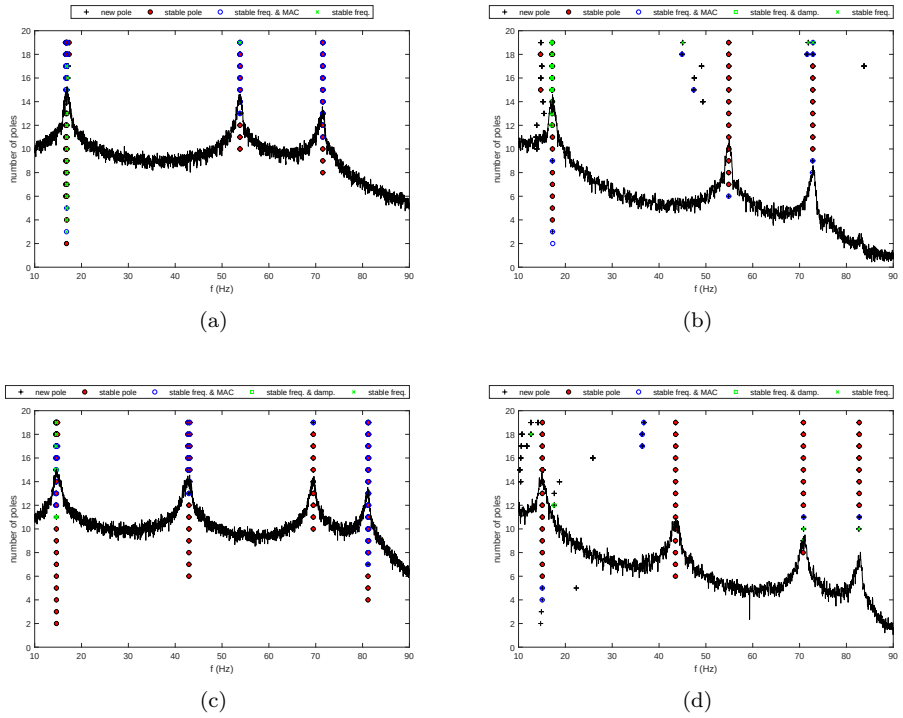

Figure 6: Stochastic Subspace Identification (SSI): stabilization diagrams for undamaged and damaged structure from acceleration (a,c) and displacement (b,d) measurements.

to automatically evaluate changes in the structural response without computing any modal parameters and the other approach requires modal parameter and their confidence intervals estimate. Also in our work, the methods used are classified in two main categories: dynamic response-based and modal-based techniques. The first techniques are based on the analysis of the dynamic response of structure in the time domain (e. g. displacements and accelerations), and they allow a real time assessment of structural conditions; the second ones require the identification of modal properties (frequencies and mode shapes) of structures (frequency domain).

4.1. Damage Location

As previously described, the determination of the position of damage in the structure can be pursued by methods belonging to the cited categories. Both approaches are followed to evidence the effects in the studied case of measurements derived by image processing.

4.1.1. Techniques based on the dynamic response in the time domain

In some cases, as for example during seismic events, it is essential to identify in real-time possible modifications of the structural response due to occurrence of damages. Therefore, time-based identification methods have been investigated by several researchers ([31], [32]) as they do not require prolonged acquisition time. These techniques make use of the response under excitation in order to identify structural damages. Dynamic measurements include structural displacements, accelerations, or strains. In this context, the use of high-speed camera offers the advantage of a direct measurement of displacement without the need of integrating twice the acceleration to obtain a direct measurement of the displacement. Based on displacement measurements, an effective damage index is the inter-storey drift, i.e. the difference between deflections of two adjacent floors. This measure has been previously employed to estimate the overall damage of a building during earthquake-like induced vibrations (see [33]). The inter-storey drift can be evaluated following three approaches: the maximum absolute storey deflection, the storey deflection when the maximum deflection at top level occurs, and the total maximum storey drift at each level considering all time-steps. [34]

In the present paper, all three approaches were evaluated but the second gave the most accurate results and so is described in the following. Let $t_{\max}$ the time instant at which the maximum displacement at the top floor occurs. The corresponding deflection of undamaged and damaged structures is shown in Fig.7.

At each measurement point i, the inter-storey drift d_i (Fig.8a) is evaluated

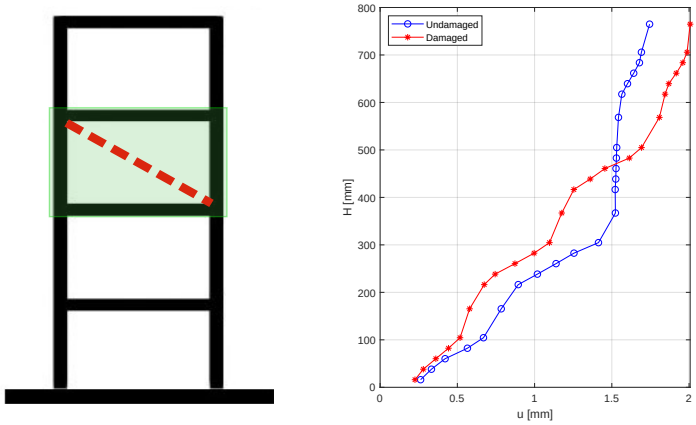

(a) (b)

Figure 7: Time-based damage identification methods: (a)area of the structure, evidenced in green, interested by the damage; (b) maximun deflection of the structure recorded at $t = t_{\max}$.

by:

$$d_i = u_i - u_{i-1} \quad \text{for} \quad i = 2, ..., N \quad \text{and} \quad d_1 = u_1 \tag{1}$$

where u_i is the displacement at measurement point i (the deflection of the structure) at $t = t_{\max}$ and N is the number of the measurement points, e.g., $N = 24$ for image processing data. The damage can be localized on the points i which maximizes the Drift Variation (DV) defined as:

$$\mathrm{DV}(i) = \frac{d_i^d - d_i^u}{d_i^u} \tag{2}$$

where d_i^u and d_i^d are the inter-storey drift of the undamaged and damaged structure respectively. The results in Fig. 8b shows that the highest values of the DV are located at an height between $400 \div 600$ mm which actually coincides with the inter-storey 2-3 where the steel bracings were removed.

The large amount of measurement points made available through the image analysis technique allowed us to evaluate the curvature of the deflection profile (Fig. 8c) of the structure and to use the Curvature Variation (CV) as an

additional damage index. As such, we have defined:

$$\mathrm{CV}(i) = \frac{\chi_i^d - \chi_i^u}{\chi_i^u}, \quad i = 1, ..., N \tag{3}$$

as the difference between the second derivative of the deflection for the undamaged χ_i^u and damaged χ_i^d specimen.

Fig.8d shows also the CV is localized in the region where damage occurred. However, when compared to DV the damage is concentrated on a narrow region.

4.1.2. Techniques based on modal properties in the frequency domain

Damage indices based on the use of mode shapes have attracted a great deal of attention since the early eighties. The basic concept is to identify and locate damage by relying on changes, between damaged and undamaged state, of mode shapes or their derivatives. The accuracy in mode shape estimate made possible by large number of measurement points available through DIC favours modal shapes and modal curvatures based identification techniques.

To this purpose, the RD (Relative Difference) index [35], based on the comparison between the undamaged ϕ_{ij}^u and damaged ϕ_{ij}^d modal shapes is introduced as:

$$\mathrm{RD}(ij) = \frac{\phi_{ij}^u - \phi_{ij}^d}{\phi_{ij}^u}, \qquad i = 1, ..., N \qquad j = 1, ..., L \tag{4}$$

where L is the number of identified modes and N the number of measurement points. The damage is identified at those location where RD overcomes a certain threshold. In this formulation, the mass is taken known and the mode shapes are normalized to unity with respect to the mass matrix ($\Phi^{\mathrm{T}} M\, \Phi = I$).

Another damage indicator widely used in literature is the COMAC (COordinate Modal Assurance Criteria) [36] defined by:

$$\mathrm{COMAC}(i) = \frac{\left(\sum_{j=1}^{L} |\phi_{ij}^d\, \phi_{ij}^u|\right)^2}{\sum_{j=1}^{L} \left(\phi_{ij}^d\right)^2 \sum_{j=1}^{L} \left(\phi_{ij}^u\right)^2} \tag{5}$$

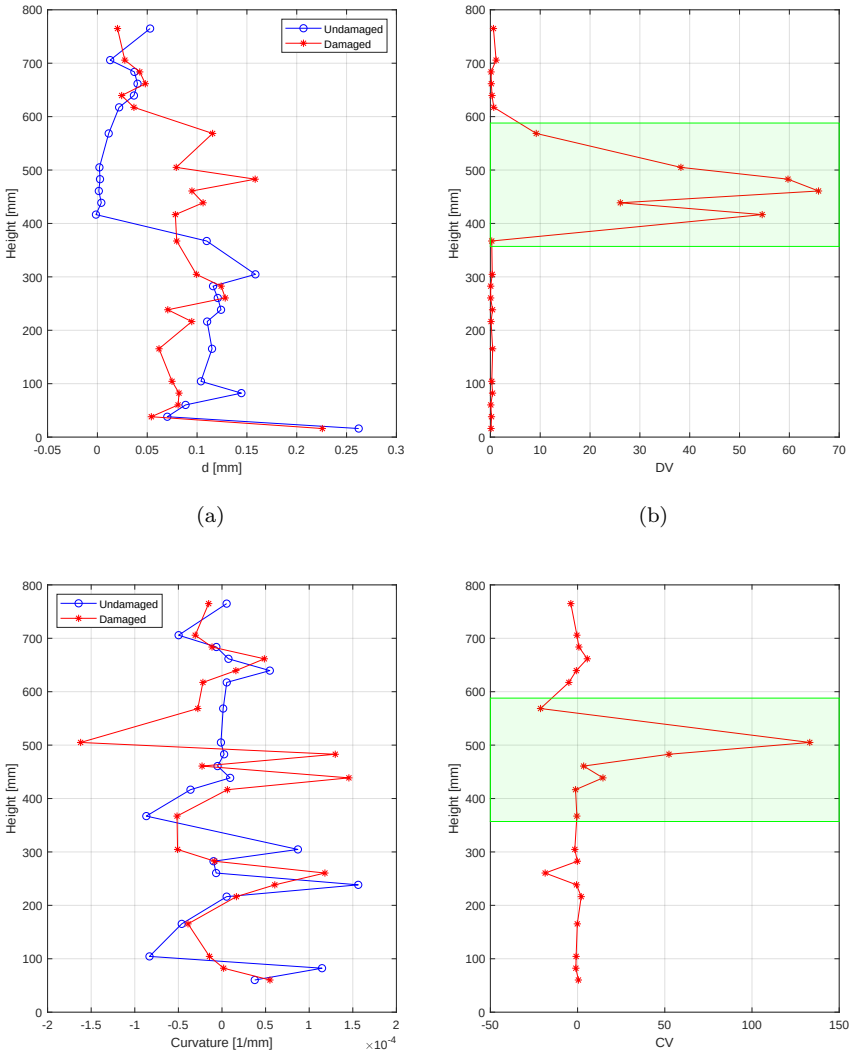

Figure 8: Time-based damage identification methods: (a) inter-storey drift at $t = t_{\max}$; (b) inter-storey Drift Variation at $t = t_{\max}$; (c) curvature at $t = t_{\max}$;(d) Curvature Variation at $t = t_{\max}$.

where again the mode shapes are normalized to mass. Differently from RD, the damage occurs in correspondence of those inidces where the COMAC is lower.

In Fig.9 both the RD and COMAC indices are evaluated for the mode shapes obtained for the acceleration data ($N = 4$) and the displacement data ($N = 24$). When considering the RD index, acceleration and displacement data gave the similar results only for the first mode for which the maxima are obtained at the same location (see the blue and the red bars in Fig.9a). For the second and third mode the maximum absolute value of RD evaluated with displacement measurements is located in the range $600 \div 700$ mm, while the maximum values of RD evaluated with acceleration measurements are in the range $350 \div 600$ mm. In all cases, RD index failed to provide a clear indication of the damage position. The minimum values of COMAC are in the range $350 \div 600$ for acceleration measurements while for the displacement ones there are three local minima in the range $350 \div 800$ where also two maxima appear. It is noted that the large number of measurement points offered by image analysis does not provide any significant advantage in terms of damage localization when compared to the few measurement points of the acceleration data.

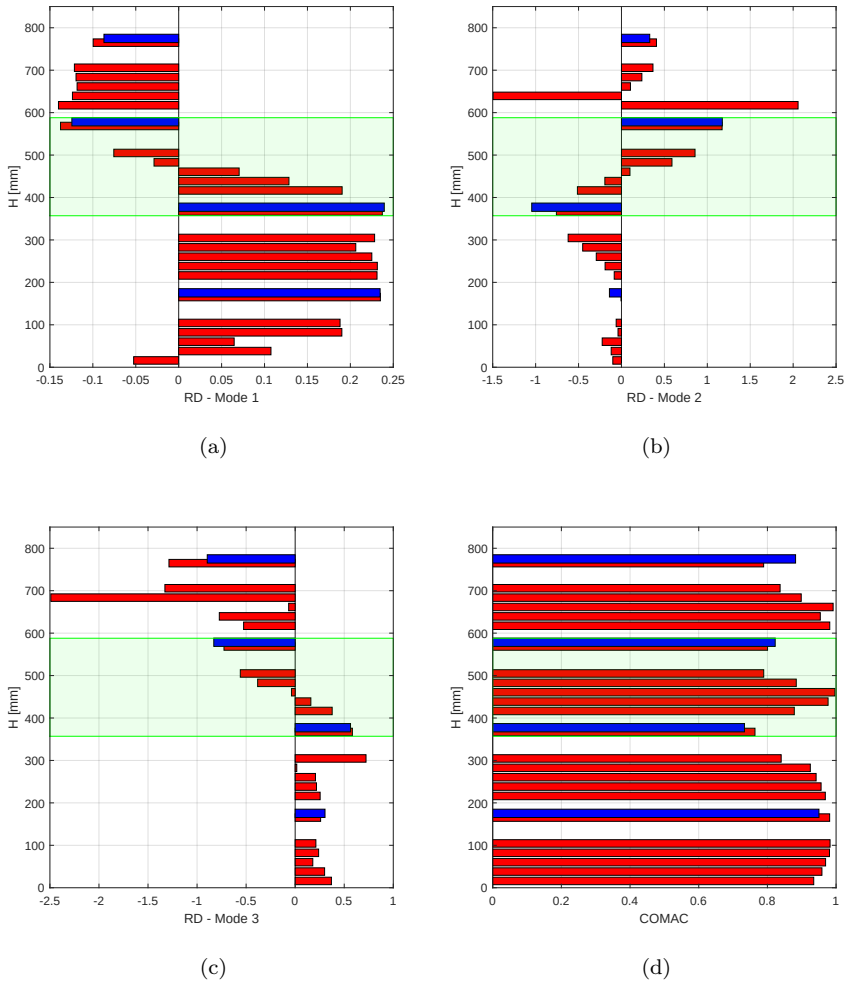

Figure 9: Relative Difference (a,b,c) and COordinate Modal Assurance Criteria (d) evaluated with acceleration (blue) and displacement (red) measurements.

Another parameter often evaluated in damage detection algorithm is the Curvature Variation (CV) of the mode shape profiles. Maximum CV are located in the damage region whereas RD are often spread all over the structure; for this reason CV are often considered a superior damage indicator. In Fig.10 is reported the CV of the mode shape profiles. The highest values of the CV are located in the range $400 \div 600$ mm for the mode shapes 1 and 2, while the CV

of mode shape 3 has high values in the range $400 \div 800$ mm. Yet in all cases, the maximum variations is obtained in the damaged region at least for lower order modes. For higher modes, CV have spurious peaks which have to be filtered out ([37], [38]).

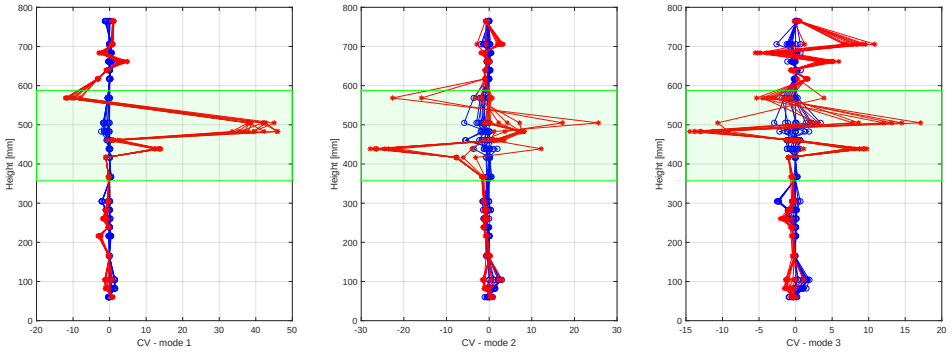

(a) (b) (c)

Figure 10: Modal curvature-based approach applied to displacement measurements: Curvature Variation of mode 1 (a), mode 2 (b), mode 3 (c). In blue the undamaged state and in red the damaged one.

For shear buildings, a specific identification procedure was proposed in [39] and [40]. This approach makes use the damage-induced deflections estimated by modal flexibility from ambient vibration measurements. This method consists in three steps. The first one is the evaluation of the modal flexibility $\mathbf{G}_m$ from natural frequencies and mass-normalized mode shapes; the second step consists in the evaluation of the deflection profile under a positive shear inspection load ($\mathbf{u} = \mathbf{G}_m \mathbf{f}$, where $\mathbf{u}$ is the displacement vector corresponding to the positive shear inspection load vector $\mathbf{f} = \{1\}$). The last step is the damage localization using the damage-induced deflections. As showed in [39], the damage-induced deflections, which occurs at the damaged floor [39]. The following index Z, based on a statistical approach, is utilized:

$$Z(i) = \frac{d_i^d - \overline{d_i^u}}{\sigma(d_i^u)} \quad \text{for} \quad i = 1, ..., N \tag{6}$$

where d_i^d is the inter-story drift of damaged structure, d_i^u is the undamaged inter-story drift, $\overline{d_i^u}$ and $\sigma(d_i^u)$ are the mean value and the standard deviation of d_i^u. The damage localization is performed using the condition $Z(i) > Z^{\text{Threshold}}$.

Fig.11 shows the Z-index for both acceleration and displacement measurements. The signals recorded during the test performed on the undamaged structure was divided in 10 intervals; at each interval, natural frequencies, mode shapes and deflection profile under a positive shear inspection were evaluated. Then, the mean value and the standard deviation of d_i^u were computed, by considering the undamaged state data as a training data set.

The maximum values of the Z index occur in the range $400 \div 600$ mm of the height of the structure that corresponds to the zone where the steel bracings have been removed. Both measurements return a good estimate of damage localization but thanks to the larger number of measurement points provided by image analysis it is possible to assess that the damage affects all the zone between 400 and 600 mm, while with the acceleration acquisition system it is possible to individuate only one point affected by damage (corresponding to the sensor on the third floor).

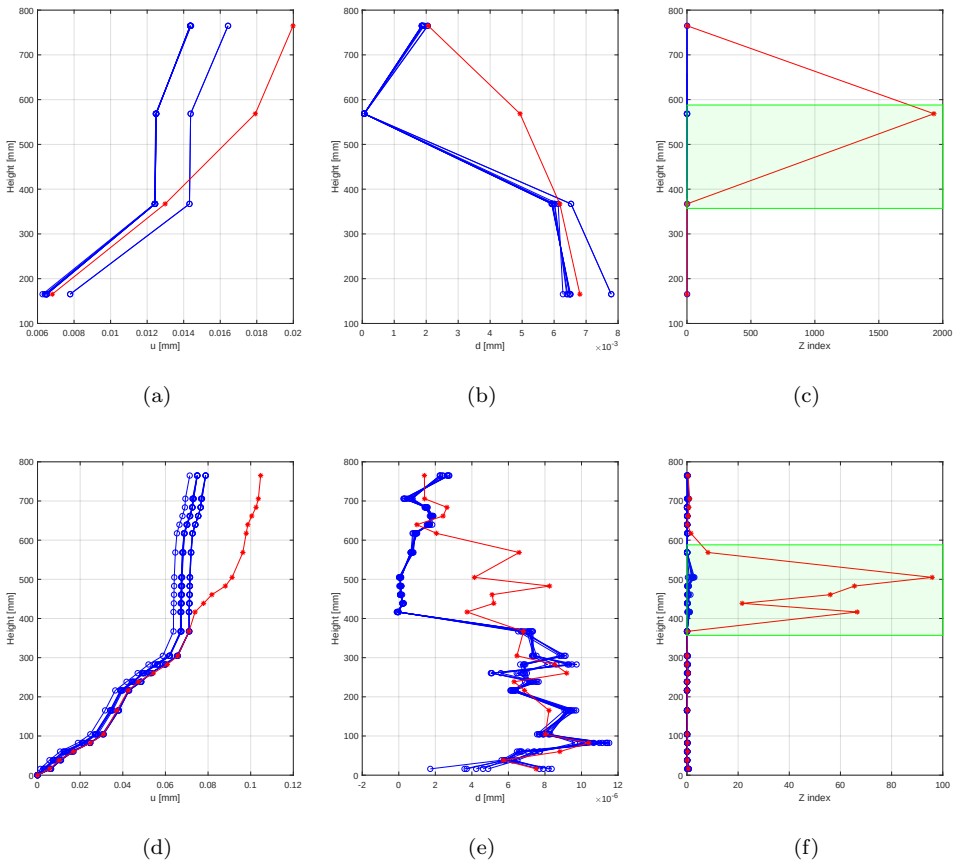

Figure 11: Modal flexibility-based approach applied to acceleration (a, b, c) and displacement (d, e, f) measurements: deflection (a,d), inter-storey drift (b,e), Z index (c,f). In blue the undamaged state and in red the damaged one.

In Fig.12 is reported the CV of the deflection profile obtained with the modal-flexibility approach. The highest values of the CV are located in the range $400 \div 600$ mm for the case of deflection profile.

Consequently, the CV damage index is more accurate if applied to the actual deflection profile for an assigned instant of time (Fig.**??**d) and to the deflection profile obtained with the modal flexibility approach (Fig.12c), rather than to the mode shapes profile (Fig.10).

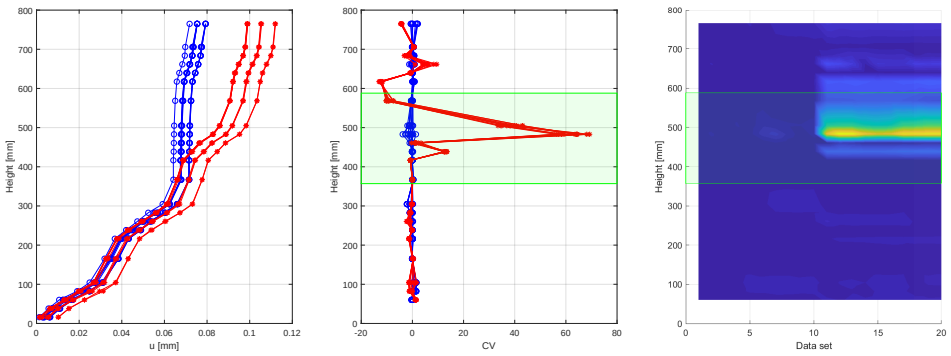

(a) (b) (c)

Figure 12: Modal flexibility-based approach applied to displacement measurements: deflection (a), Curvature Variation of the deflection profile (b), Curvature Variation in time (c). In blue the undamaged state and in red the damaged one.

In order to give an overview of the effectiveness of each damage index a summary of the results is presented in Tab.3. The indices which correctly locate the damage position are indicated with the check mark "$\surd$", whereas those with a "x" did not provide the correct result. The symbol "-" is used when it was not possible to calculate the indicator with that type of measurements. The direct displacement measurements allow to use techniques based on the deformation of the structure at a certain instant of time and those based on the variation of curvature. The RD and COMAC indices give better results in the case of accelerometric measurements, while the drift-based indices are able to localize the damage both by accelerometric and displacement measurements but with the latter a more accurate localization was obtained.

4.2. Damage Intensity

The methods described in the previous section allow the localization of damage. In this section, those results are used to solve the inverse problem related to the esimate of the damage intensity. Such an approach requires numerical model of the structure and a comparison between its undamaged and damaged state; as

Table 3: Summary and comparison of the results of damage location indicators.

	Accelerations	Displacements
Techniques based on the dynamic response in the time domain		
Deflection profile at $t = t_{max}$	-	√
▷ Inter-storey Drift Variation (DV)	-	√
▷ Curvature Variation (CV)	-	√
Techniques based on modal properties in the frequency domain		
Mode shapes	√	√
▷ Relative Difference (RD)	√	x
▷ Coordinate Modal Assurance Crit. (COMAC)	√	x
▷ Curvature Variation (CV)	-	√
Modal flexibility-based approach	√	√
▷ Inter-storey drift variation (Z index)	√	√
▷ Curvature Variation (CV)	-	√

such, two numerical models of the shear-type frame structure have been implemented, a 4-DOFs and a 24-DOFs modal model (Fig.13) to assess the damage intensity by using, respectively, accelerometer and image-based measurements. The first model was obtained by recognizing 4 significant DOFs in the structure, which are the 4 horizontal translations of each floor for the shear-type frame; the second model was implemented with 24 DOFs that correspond to 6 nodes for each floor (5 on the column and 1 in correspondence with the beam), in analogy to the displacement measurement points. These models were used to evaluate the natural frequencies f_j and to extract the corresponding mode shapes.

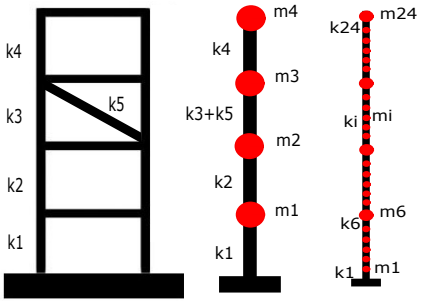

Figure 13: The shear-type frame structure in the undamaged configuration, the 4-DOFs and 24-DOFs model.

After identifying the location of the damage by selecting the area where the indices reported in the previous section exceed a fixed threshold, the damage is introduced in the model with a stiffness reduction of the elements which are situated in the localization area. The stiffness k_i^d of the element i interested by the damage can be expressed in relation to the stiffness of the element undamaged, k_i^u, as follows:

$$k_i^d = (1-a)\, k_i^u, \quad i = 1, ..., n \tag{7}$$

where a is the damage intensity, i.e. $0 \leq a < 1$ and n is the number of the elements ($n = 4$ for 4-DOFs model, $n = 24$ for 24-DOFs model).

The estimate of the parameter a constitutes the assessment of the damage intensity. An optimal estimate of this parameter can be obtained by minimizing an objective function based on the sum of difference between numerical $\Delta f_j(a)$ and experimental Δf_{ej} frequencies variation from undamaged to damaged state, i.e.,

$$G(a) = \sum_{j=1}^{L} \left(\frac{\Delta f_j(a)}{f_j^u} - \frac{\Delta f_{ej}}{f_{ej}^u} \right)^2 \tag{8}$$

where L denotes the number of the identified modes, $\Delta f_j(a) = f_j^u - f_j^d(a)$ and $\Delta f_{ej} = f_{ej}^u - f_{ej}^d$.

The G function is calculated in Fig.14 for experimental frequencies obtained from accelerometer and image-based measurements after having identified the

location of the damage with the methods previously presented. The actual damage intensity is represented with a vertical dashed line. In this figure, they are classified differently from the classification of the previous section. In Fig.14a is reported the objective function coming from a pre-localization of the damage based on drift variation: DV at t_{max} (Fig.8b) and Z index from modal flexibility-based approach (Fig.11c,f). In Fig.14b the pre-localization is obtained with curvature variation indices: CV at t_{max} (Fig.8d), CV of mode shapes Fig.10 and CV from modal flexibility-based approach (Fig.12b). Fig.14c,d report the results coming from a damage located with COMAC (Fig.9d) and RD (Fig.9a,b,c) index, respectively.

These results show that the only the damage indices based on drift variation (14a) allow to obtain a good assessment of damage intensity: only in this case, in fact, the value of the parameter a that minimize of $G(a)$ coincides with the actual value of the a (indicated by the dashed line). In all other cases, the stiffness reduction is underestimated by at least 15%.

5. Conclusions

In this work, two vision-based techniques were used to measure the dynamic displacements of a small-scale frame structure and to extract its modal properties. The advantages of the image-based techniques were exploited in a damage detection problem, in which the damage was introduced by removing the two steel bracing located on the third floor of the frame. The damage intensity was assessed by solving the inverse problem formulated in terms of either displacement or accelerations.

The results showed that the increased number of points available by image analysis allow a more accurate assessment damage position, both for techniques based on the dynamic response in time domain and on modal properties in the frequency domain. The vision-based monitoring allows to use techniques which are not applicable to the measurements coming from the accelerometer based acquisition system, such as the techniques applied to the deformation

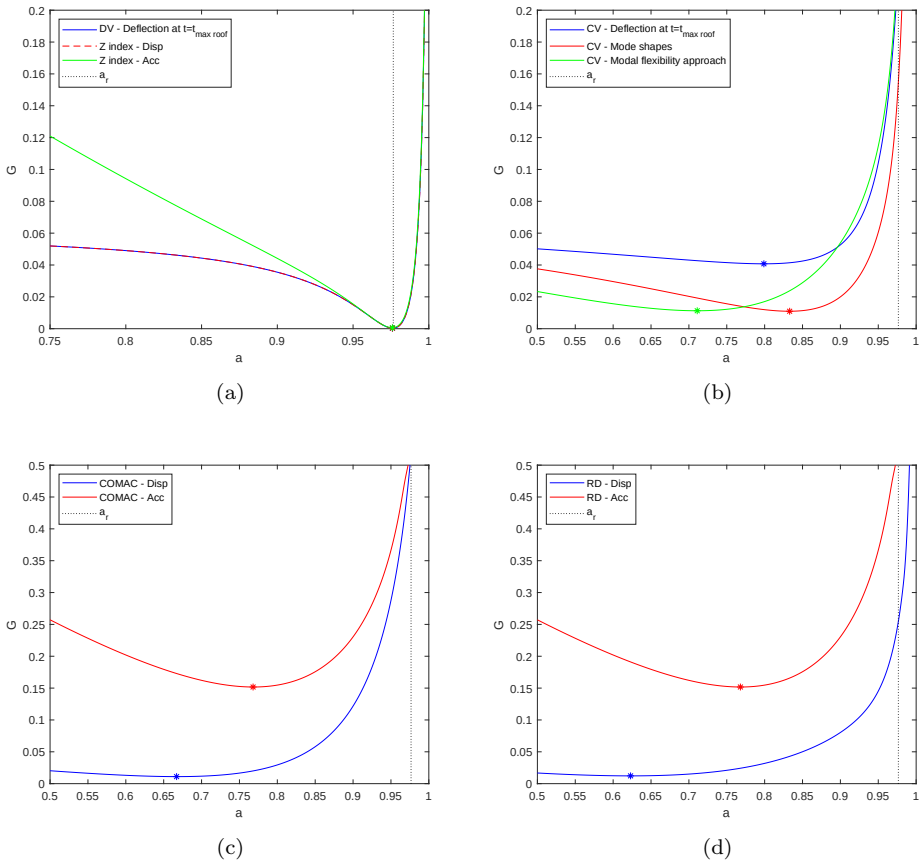

Figure 14: The objective function $G(a)$ calculated with experimental frequencies obtained from accelerometer (Acc) and image-based (Disp) measurements after identifying the location of the damage with different methods, based on drift variation (a), curvature variation (b), COMAC (c) and RD (d).

of the structure at a certain instant of time, because with image analysis we obtained direct displacement measurements, and those based on curvature variation thanks to the high number of measurement points. Other techniques were applied both to accelerometric and displacement measurements. Among them, the Z index evaluated with the modal flexibility-based approach is able to localize the damage with both data but with the image analysis data a more accurate localization was obtained. Only the RD and COMAC indices give better results in the case of accelerometric measurements; in this case the high number of sampling points in the images returns several false positive.

The damage intensity was assessed with a procedure based on the pre-localization of the damage and on the definition of an inverse problem, which requires the implementation of a numerical model of the structure. The damage intensity has been estimated by minimizing an objective function based on the sum of difference between numerical and experimental frequencies variation from undamaged to damaged state. The results show that, among all the techniques used for damage localization, only two (Z index and DV) allow to achieve a good assessment of damage intensity. This is due to the good estimate of damage position obtained with these indices which are based both on drift variation. Z index was be applied to both accelerometer and image-based measurements and allowed to estimate damage intensity with the same accuracy. Whereas it was possible to apply DV only to image-based data which are direct displacement measurements.

In conclusion, in the damage localization task, the image analysis data allowed to obtain better results in terms of accuracy and in term of quantity of techniques usable; in the damage intensity task, the advantages of the image data reside in the higher quantity of techniques usable.

Acknowledgments

This work is part of a project that has received funding from the Research Fund for Coal and Steel under grant agreement No 800687.

References

[1] X. W. Ye, C. Z. Dong, T. Liu, A review of machine vision-based structural health monitoring: Methodologies and applications, Journal of Sensors 2016 (2016).

[2] J. G. Chen, N. Wadhwaa, Y. J. Cha, F. Durand, W. T. Freeman, O. Buyukozturk, Modal identification of simple structure swith high-speed video using motion magnification, Journal ofSoundandVibration 345 (2015) 58–71.

[3] C. Dong, F. Catbas, A review of computer vision–based structural health monitoring at local and global levels, Structural Health Monitoring 20(2) (2020) 692–743.

[4] J. Guo, J. Jiao, K. Fujita, I. Takewaki, Damage identification fcr stnxtures using vision-based measurement, Engineering Structures 199, 109634 (2019).

[5] J. Yoshida, M. Abe, S. Kumano, Y. Fujino, Construction of a measurement system for the dynamic behaviors of membrane by using image processing, Structural Membrane (2003) 576–579.

[6] P. Olaszek, Investigation of the dynamic characteristic of bridge structures using a computer vision method, Measurement 25(3) (1999) 227–236.

[7] H. Yoon, H. Elanwar, H. Choi, M. Golparvar-Fard, B. F. S. Jr., Target-free approach for vision-based structural system identification using consumer-grade cameras, Structural Control and Health Monitoring 23 (2016) 1405–1416.

[8] C. Harris, M. Stephens, A combined corner and edge detector, in: Alvey vision conference, 1988. Manchester, UK.

[9] C. Tomasi, T. Kanade, Detection and tracking of point features, in: School of Computer Science, Carnegie Mellon Univ: Pittsburgh, 1991.

[10] Y. Xu, Photogrammetry-based structural damage detection by tracking a visible laser line, Structural Health Monitoring 19(1) (2020) 322–336.

[11] A. Havaran, M. Mahmoudi, Extracting structural dynamic properties utilizing close photogrammetry method, Measurement 150 (2020) 107092.

[12] Y. Yang, C. Dorn, T. Mancini, Z. Talken, G. Kenyon, C. Farrar, D. Mascareñas, Blind identification of full-field vibration modes from video measurements with phase-based video motion magnification, Mechanical Systems and Signal Processing 85 (2017) 567–590.

[13] Y. F. Ji, C. C. Chang, Nontarget image-based technique for small cable vibration measurement, Journal of Bridge Engineering 13(1) (2008) 34–42.

[14] S. Patsias, W. J. Staszewskiy, Damage detection using optical measurements and wavelets, Structural Health Monitoring 1(1) (2002) 5–22.

[15] U. P. Poudel, G. Fu, J. Ye, Structural damage detection using digital video imaging technique and wavelet transformation, Journal of Sound and Vibration 286(4-5) (2005) 869–895.

[16] D. M. McCarthy, Monitoring 3d vibrations in structures using high resolution blurred imagery, Ph.D. thesis, School of Civil and Building Engineering Loughborough University (2015).

[17] G. Boracchi, V. Caglioti, A. Giusti, Ball position and motion reconstruction from blur in a single perspective image, in: Image Analysis and Processing, 2007. ICIAP 2007. 14th International Conference, IEEE Comput. Soc., Iciap, Modena.

[18] D. M. J. McCarthy, J. H. Chandler, A. Palmeri, Monitoring dynamic structural tests using image deblurring techniques, Key Engineering Materials (2013) 932–939.

[19] C. Z. Dong, F. N. Catbas, A review of computer vision–based structural health monitoring at local and global levels, Structural Health Monitoring 20(2) (2020) 692–743.

[20] B. Pan, L. Tian, X. Song, Real-time, non-contact and targetless measurement of vertical deflection of bridges using off-axis digital image correlation, Ndt & E International 79 (2016) 73–80.

[21] A. Khaloo, D. Lattanzi, Pixel-wise structural motion tracking from rectified repurposed videos, Structural Control and Health Monitoring 24(11) (2017) e2009.

[22] H. Yoon, H. Elanwar, H. Choi, M. Golparvar-Fard, B. F. Spencer Jr, Target-free approach for vision-based structural system identification using consumer-grade cameras, Structural Control and Health Monitoring 23(12) (2016) 1405–1416.

[23] C. Rinaldi, J. Ciambella, M. Moroni, V. Gattulli, Optical flow dynamic measurements with high-speed camera on a small-scale steel frame structure, Carcaterra A., Paolone A., Graziani G. (eds) Proceedings of XXIV AIMETA Conference 2019. AIMETA 2019. Lecture Notes in Mechanical Engineering (2020) 1543–1555.

[24] M. Moroni, A. Cicci, M. Bravi, Experimental investigation of a local recirculation photobioreactor for mass cultures of photosynthetic microorganisms, Water Research 52 (2014) 29–39.

[25] S. Yoneyama, G. Murasawae, Digital image correlation, in: Experimental Mechanics; Freire, J.F., Ed.; Encyclopedia of Life Support System (EOLSS) Publishers: Oxford, UK, 2009.

[26] D. Foti, V. Gattulli, F. Potenza, Output-only identification and model updating by dynamic testing in unfavorable conditions of a seismically damaged building, Computer-Aided Civil and Infrastructure Engineering 29(9) (2014) 659–675.

[27] E. Antonacci, A. D. Stefano, V. Gattulli, M. Lepidi, E. Matta, Comparative study of vibration-based parametric identification techniques for a three-

dimensional frame structure, Journal of Structural Control and Health Monitoring 19(5) (2012) 579–608.

[28] R. Brincker, L. Zhang, P. Andersen, Modal identification of output-only systems using frequency domain decomposition, Smart Materials and Structures 10 (2001) 441–445.

[29] B. Peeters, G. D. Roeck, Stochastic system identification for operational modal analysis: a review, Journal of Dynamic Systems, Measurement, and Control 123(4) (2001) 659–667.

[30] M. Döhler, F. Hille, L. Mevel, W. Rücker, Structural health monitoring with statistical methods during progressive damage test of s101 bridge, Engineering Structures 69 (2014) 183–193.

[31] J. Cattarius, D. J. Inman, Time domain analysis for damage detection in smart structures, Mechanical Systems and Signal Processing 11(3) (1997) 409–423.

[32] M. Vafaei, A. B. Adnan, A. B. A. Rahman, Real-time seismic damage detection of concrete shear walls using artificial neural networks, Journal of Earthquake Engineering 17(1) (2013) 137–154.

[33] M. Celebi, A. Sanli, M. Sinclair, S. Gallant, D. Radulescu, Real-time seismic monitoring needs of a building owner—and the solution: A cooperative effort, Earthquake Spectra 20(2) (2004) 333–346.

[34] A. S. Hokmabadi, B. Fatahi, B. Samali, Recording interstorey drifts of structures in time-history approach for seismic design of building frames, Australian Journal of Structural Engineering 13(2) (2012) 175–180.

[35] C. H. J. Fox, The location of defects in structures. a comparison of the use of natural frequency and mode shape data, 10th International Modal Analysis Conference, IMAC (1992).

[36] N. A. J. Lieven, D. J. Ewins, Spatial correlation of mode shapes, the coordinate modal assurance criterion (comac), 6th International Modal Analysis Conference, IMAC (1998).

[37] J. Ciambella, F. Vestroni, The use of modal curvatures for damage localization in beam-type structures, Journal of Sound and Vibration 340 (2015) 126–137.

[38] J. Ciambella, A. Pau, F. Vestroni, Modal curvature-based damage localization in weakly damaged continuous beams, Mechanical Systems and Signal Processing 121 (2019) 171–182.

[39] K.-Y. Koo, S. H. Sung, J. W. Park, H. J. Jung, Damage detection of shear buildings using deflections obtained by modal flexibility, Smart materials and structures 19(11) (2010).

[40] G. Bernagozzi, S. Mukhopadhyay, R. Betti, L. Landi, P. P. Diotallevi, Output-only damage detection in buildings using proportional modal flexibility-based deflections in unknown mass scenarios, Engineering Structures 167 (2010) 549–566.